International Journal of Heat and Mass Transfer 53 (2010) 5605–5621

Contents lists available at ScienceDirect

International Journal of Heat and Mass Transfer

journal homepage: www.elsevier.com/locate/ijhmt

Subcooled flow boiling heat transfer and associated bubble characteristics of FC-72 on a heated micro-pin-finned silicon chip

W.R. Chang, C.A. Chen, J.H. Ke, T.F. Lin *

Department of Mechanical Engineering, National Chiao Tung University, Hsinchu, 1001 Ta Hsueh Road, Hsinchu 30010, Taiwan

ARTICLE INFO

Article history:
Received 6 November 2009
Received in revised form 16 April 2010
Accepted 16 April 2010
Available online 2 August 2010

Keywords:
Subcooled flow boiling
FC-72
Micro-pin-fins
Bubble characteristics

ABSTRACT

Experiments are conducted here to investigate subcooled flow boiling heat transfer and associated bubble characteristics of FC-72 on a heated micro-pin-finned silicon chip flush-mounted on the bottom of a horizontal rectangular channel. In the experiments the mass flux is varied from 287 to 431 kg/m^2 s, coolant inlet subcooling from 2.3 to 4.3 °C, and imposed heat flux from 1 to 10 W/cm^2. Besides, the silicon chips contain three different geometries of micro-structures, namely, the smooth, pin-finned 200 and pin-finned 100 surfaces. The pin-finned 200 and 100 surfaces, respectively, contain micro-pin-fins of size 200 μm × 200 μm × 70 μm (width × length × height) and 100 μm × 100 μm × 70 μm. The measured data show that the subcooled flow boiling heat transfer coefficient is reduced at increasing inlet liquid subcooling but is little affected by the coolant mass flux. Besides, adding the micro-pin-fin structures to the chip surface can effectively raise the single-phase convection and flow boiling heat transfer coefficients. Moreover, the mean bubble departure diameter and active nucleation site density are reduced for rises in the FC-72 mass flux and inlet liquid subcooling. Increasing coolant mass flux or reducing inlet liquid subcooling results in a higher mean bubble departure frequency. Furthermore, larger bubble departure diameter, higher bubble departure frequency, and higher active nucleation site density are observed as the imposed heat flux is increased. Finally, empirical correlations for the present data for the heat transfer and bubble characteristics in the FC-72 subcooled flow boiling are proposed.

1. Introduction

In recent quick development of the IC (Integrated Circuits) technology, novel design in many electronic devices increases their power density and hence results in more heat dissipation for the same device size, especially for the advanced microprocessors and high power modules. As denoted by Simons [1], the IC junction temperature must be kept under 85 °C to avoid being damaged. The heat removal methods based on the traditional air-cooling are normally insufficient for these high power density requirements. Due to high ability in the heat transfer rate, two-phase flow boiling is considered as one of the most effective methods in electronics cooling. To ensure safety and stability of the cooling, dielectric coolant FC-72 made by 3M Company satisfies the above essentials and has been studying for the electronics cooling in recent years. Besides, the use of surface micro-structure to enhance the heat transfer performance is expected to be beneficial. Thus, it becomes increasingly important to understand the flow boiling processes of the dielectric liquid on micro-structure enhanced surfaces and the associated heat transfer. Moreover, boiling heat transfer in subcooled liquid flow is known to be better than in saturated liquid. However, heat transfer and associated bubble characteristics in subcooled flow boiling of FC-72 on various microstructure surfaces remain largely unexplored.

In the following the literature relevant to the present study is reviewed. Mudawar and his colleague [2] experimentally studied the subcooled flow boiling of FC-72 on a linear array of discrete heat sources in a vertical channel for the flow velocity ranging from 13 to 400 cm/s. They found that the boiling incipience was delayed to higher heat flux values for a higher flow velocity. Similar experiments for a horizontal heat source array were conducted by Heindel et al. [3]. They noted that an increase in the flow velocity caused reduction of temperature overshoot at onset of nucleation boiling (ONB) but exhibited little effect on the boiling curves in the fully developed nucleate boiling region. As the liquid subcooling increases, the temperature overshoot at ONB decreases and the surface heat flux increases. Similarly, Tso et al. [4] found that the chip surface temperature decreased with the increases of the flow velocity and liquid subcooling only in the partial boiling region. Samant and Simon [5] analyzed the heat transfer from a small region to refrigerants R-113 and FC-72 and noted that as the flow velocity and subcooling increased, the temperature excursion and boiling hysteresis appeared less pronounced.

* Corresponding author.
E-mail address: tfiln@mail.nctu.edu.tw (T.F. Lin).

0017-9310/$ - see front matter © 2010 Published by Elsevier Ltd.
doi:10.1016/j.ijheatmasstransfer.2010.05.014

Nomenclature

A_f	surface area of a single fin (m^2)
A_s	surface area of a bare chip (m^2)
Bo	Boiling number, $Bo = \frac{q''}{G \cdot i_{lv}}$, dimensionless
c_p	specific heat (J/kg °C)
D_h	hydraulic diameter of rectangular channel (m)
E	enhancement factor
$f, \bar{f}$	mean dimensional and dimesionless bubble departure frequency (s^{-1})
F	pin-fin factor for the effects of fin geometries, dimensionless
Fr_l	Froude number, $Fr_l = \frac{G^2}{\rho_l^2 \cdot g \cdot D_h}$, dimensionless
g	acceleration due to gravity (m^2/s)
G	mass flux (kg/m^2 s)
h	heat transfer coefficient (W/m^2 K)
H	height (m)
I	measured current from DC power supply (A)
i_{lv}	enthalpy of vaporization (J/kg K)
Ja'	Jacob number based on ΔT_{sub}, $Ja' = \frac{\rho_l \cdot c_{pl} \cdot \Delta T_{sub}}{\rho_v \cdot i_{lv}}$, dimensionless
k	thermal conductivity (W/m K)
L	length (m)
N	number of micro-pin-fins
N_{ac}	Active nucleation site density (n/m^2)
N_{conf}	Confinement number, $N_{conf} = \frac{(\sigma/(g \cdot \Delta\rho))^{0.5}}{D_h}$, dimensionless
Nu	Nusselt number, $Nu = \frac{h \cdot L}{k}$, dimensionless
P	system pressure (kPa)
Pr	Prandtl number, $Pr = \frac{\mu \cdot c_p}{k}$, dimensionless
Q	heat transfer rate (W)
q''	average imposed heat flux (W/cm^2)
Re_l	liquid Reynolds number, $Re_l = \frac{G \cdot D_h}{\mu_l}$, dimensionless
T	temperature (K)
$u_{l,in}$	liquid FC-72 velocity at the inlet (m/s)
V	measured voltage from DC power supply (V)

Greek symbols

ΔT	temperature difference (K)
ρ	density, kg/m^3
μ	dynamic viscosity (N s/m^2)
ε	relative heat loss, dimensionless
σ	surface tension (N/m)

Ma and Chung [6] examined bubble dynamics in reduced gravity flow boiling of FC-72 over a thin gold film semi-transparent heater. The bubble departure size was found to be bigger in the micro-gravity environment. At increasing flow rate, the bubble departure time and departure size decrease. This was also found by Situ et al. [7] later. Besides, they also noted that the bubble growth rate dropped sharply after lift-off. In addition, Yin et al. [8] examined the subcooled flow boiling of R-134a in an annular duct and found that both the bubble departure size and frequency reduced at increasing liquid subcooling. Experiments conducted by Chang et al. [9] for R-134a and water focused on the behavior of near-wall bubbles in subcooled flow boiling. They identified four different two-phase flow patterns including the discrete attached bubbles, sliding bubbles, small coalesced bubbles and large coalesced bubbles or vapor clots at increasing heat flux. For a higher mass flux of the flow, the coalesced bubbles are smaller. Bang et al. [10] further noticed the presence of the R-134a vapor remnants below the discrete bubbles and coalesced bubbles, and the presence of an interleaved liquid layer between the vapor remnants and bubbles. Besides, the bubble layer could be divided into two types – a near-wall bubble layer dominated by small bubbles and a following bubble layer prevailed by large coalesced bubbles. Using digital imaging and analyzing techniques, Maurus et al. [11] investigated subcooled flow boiling and noted that the bubble population increased with the heat flux and the bubble density reduced drastically at increasing mass flux. Besides, the bubble size increases at increasing heat flux and decreasing mass flux. In a continuing study [12] they further showed that the effects of the heat flux and mass flux on the bubble size distribution were weak for small bubbles but became more pronounced for bigger bubbles. The total bubble life time, the remaining lifetime after the detachment process, and the waiting time between two bubble cycles decrease significantly as the mass flux increases.

Flow boiling of FC-72 over microstud, microgroove, and cylindrical micro-pin-fin enhanced surfaces flush-mounted on a vertical rectangular-channel wall was examined by Maddox and Mudawar [13]. The presence of the surface micro-structures was found to significantly enhance the heat transfer performance and reduce the boiling hysteresis. Heat transfer in pool boiling of FC-72 on silicon chips with the surface micro-structures of micro-pin-fins was recently investigated by Honda et al. [14,15]. They noted that both the nucleate boiling heat transfer and the critical heat flux were effectively enhanced by the micro-pin-fins. The observed boiling phenomena revealed that a small amount of vapor was left within the gap between the pin-fins when a growing bubble left the surface. On the other hand, Honda and Wei [16] conducted a critical review on the boiling heat transfer enhanced by the surface-structures. They indicated that all the surface micro-structures including the microroughness, micro-reentrant, and microporous structures were helpful in reducing the boiling incipience superheat. Generally, the micro-pin-fins were most effective in augmenting CHF and micro-porous structures were most effective in enhancing nucleate boiling heat transfer. Recently, Ramaswamy et al. [17] examined the effects of varying geometrical parameters on boiling from microfabricated enhanced structures. They showed that increasing pore size caused higher heat dissipation and the pore pitch had more significant effect on the heat transfer performance. Finally, nucleate boiling heat transfer from the micro-porous finned surface was found to be better than the plain finned surface [18].

The above literature review clearly indicates that the pool boiling heat transfer from micro-structure surface and the associated bubble dynamics have received some attention. But heat transfer and bubble characteristics in flow boiling of dielectric coolants on micro-structure surfaces have been less explored. In a recent study [19], we conducted an experiment to investigate the saturated flow boiling of FC-72 over a micro-pin-fin surface flushed-mounted on the bottom of a horizontal rectangular channel. Here in the present study we move further to examine the subcooled flow boiling heat transfer and the associated bubble characteristics of FC-72 on the same micro-pin-fin surfaces.

2. Experimental apparatus and procedures

The present experimental system consists of a degassing unit, a coolant loop, a hot-water loop, and a cold-water loop, as schematically depicted in Fig. 1. The degassing unit is a tank of 8 l in capacity with an electric-heater in it to expel the dissolved air or non-condensable gas in the FC-72 coolant before every run. Then we remove any non-condensable gases or moisture possibly present in the coolant loop by using a vacuum pump and fill the loop with the degassed liquid FC-72. The coolant loop includes a

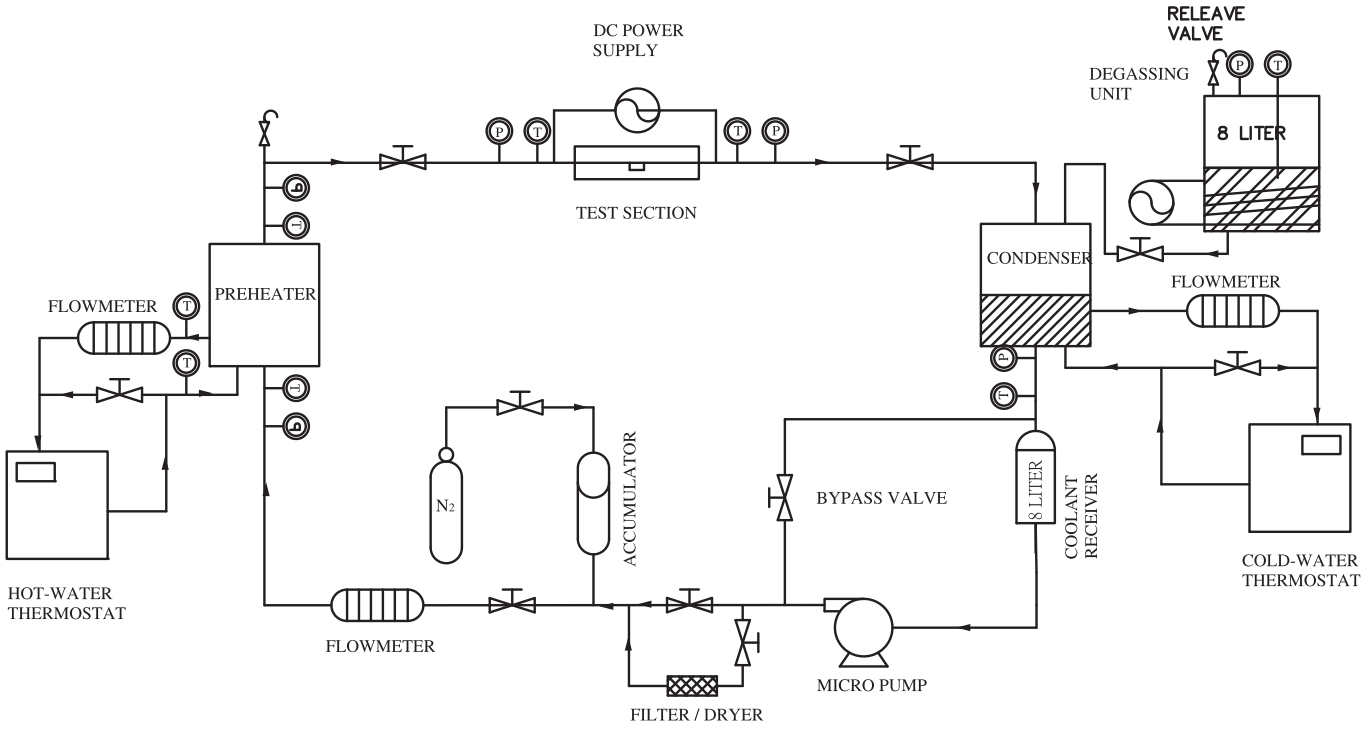

Fig. 1. Schematic diagram of experimental apparatus.

variable-speed magnetic micro-pump, filter, volume flow meter, pre-heater, test section, condenser, and receiver. The coolant flow rate is mainly controlled by the micro-pump regulated by an inverter driven AC motor. Besides, the coolant flow rate can be further adjusted by a by-pass valve. The inlet subcooled condition of the coolant FC-72 is controlled by a pre-heater unit, which exchanges heat with a water-loop thermostat. The condenser liquefies the vapor-liquid coolant mixture from the test section in the cold-water loop. All the coolant and water temperatures are measured by T-type thermocouples with a calibrated accuracy of ±0.2 °C.

The test section is a rectangular channel of 20 mm in width, 5 mm in height, and 150 mm in length with a silicon chip flush-mounted on the geometric center of the bottom plate of the channel. The flow-channel consists of a gradually converging inlet section, the main test section, and a gradually diverging exit section. An observational window is installed on the upper lid of the test section right above the chip. The silicon chip module schematically shown in Fig. 2 consists of a hollow cylindrical Teflon block, a cylindrical Teflon bolt, a silicon chip, a copper plate, two pieces of mica, a Teflon plate, and an electric-heater. To reduce the thermal contact resistance, thermal conducting grease is filled into the gaps between all the adjacent plates. The surface area of the silicon chip is 10 mm × 10 mm and the chip is heated by passing DC current through the electric-heater. Besides, three calibrated thermocouples are fixed at the back surface of the silicon chip to estimate the upper surface temperature of the chip and another calibrated thermocouple is fixed at the upper surface of the electric-heater to measure its surface temperature. The square micro-pin-fins on the silicon chip are fabricated by the semiconductor manufacturing technique. Two surface micro-structures in the form of square micro-pin-fins are manufactured on the silicon chips and each individual fin has the same size of 200 μm × 200 μm × 70 μm for the pin-finned 200 surface and 100 μm × 100 μm × 70 μm for the pin-finned 100 surface. The space between the two adjacent fins (the fin pitch) is about equal to the fin width and the detailed photographs of the arrays of the micro-pin-fins on the chips taken by an electronic microscope are shown in Fig. 3. More detailed description of the experimental system is given in the previous study [19].

Before conducting the experiments, the liquid FC-72 is degassed and then filled into the coolant receiver. Besides, the non-condensable gas in the coolant loop is evacuated. In each test, we first turn on the pump controller and set the inverter frequency to the required rotation rate of the AC motor to regulate the FC-72 flow rate to a preset level. Then the temperature and flow rate of the hot-water loop are selected so that the FC-72 temperature at the test section inlet can be maintained at a preset subcooled level. The imposed heat flux to the coolant in the test section is adjusted by varying the electric current delivered from the DC power supply. In addition, the current delivered to and voltage drop across the heater are measured. The temperature and flow rate of the cold water in the cold-water loop can be adjusted to condense the liquid–vapor mixture of FC-72 from the test section. Next, we regulate the FC-72 pressure at the test section inlet by adjusting the gate valve locating right after the test section exit. Meanwhile we use the by-pass valve to further adjust the coolant flow rate to the required level. All measurements proceed when the experimental system has reached a statistically stable state. Finally, all the data channels are scanned at an interval of 1 s for a period of 30 s.

3. Data reduction

At first, the total power input Q_t to the silicon chip can be calculated from the measured voltage drop across and electric current passing through the electric-heater, $Q_t = V \cdot I$. The imposed heat flux q'' to the coolant FC-72 in the channel is calculated on the basis of the surface area of the silicon chip and the effective power input Q_e which is directly evaluated by assuming the 1-D heat conduction across the copper and mica plates sandwiched between the silicon chip and the electric-heater by neglecting the heat loss from the side walls of the copper and mica plates,

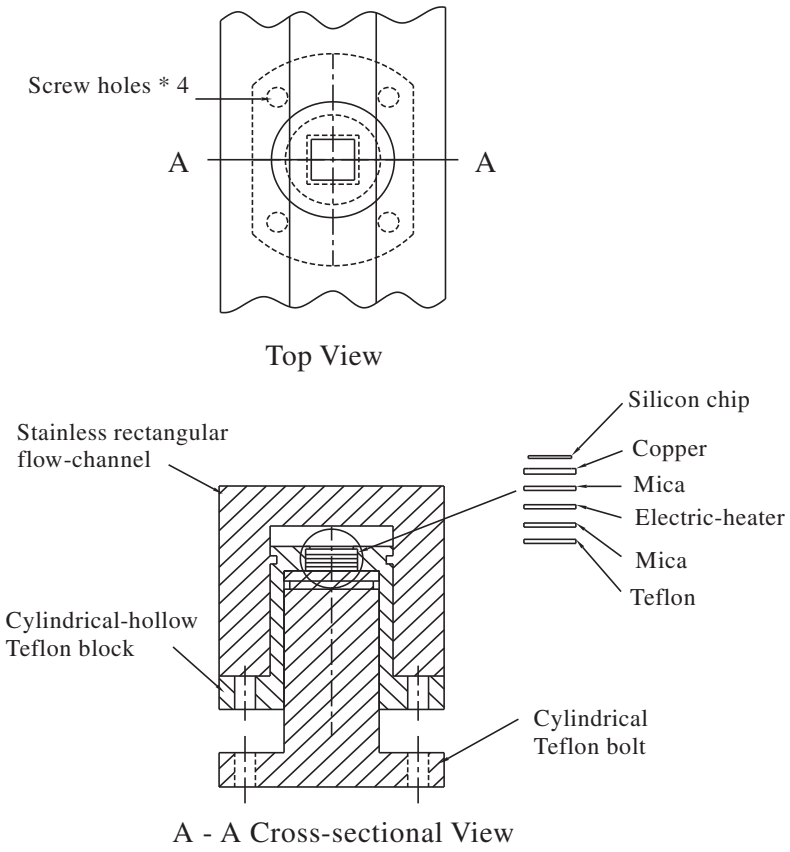

Fig. 2. Schematic of silicon chip module.

$$Q_e = \frac{\Delta T_{c,h}}{R_{c,h}} \tag{1}$$

where $\Delta T_{c,h} = T_{heater} - T'_{chip}$ is the temperature difference between the upper surface of the heater and lower surface of the chip, and $R_{c,h}$ is the total thermal resistance from the heater surface to the copper surface including the resistances of the copper and mica plates. T'_{chip} denotes the average measured temperature of the thermocouples located on the lower surface of the chip. Hence, the imposed heat flux at the chip surface is defined as

$$q'' = Q_e/A_s \tag{2}$$

where A_s is the surface area of the bare chip. The relative heat loss from the test section is defined as

$$\varepsilon = (Q_t - Q_e)/Q_t \tag{3}$$

In the present experiments the relative heat loss is found to be less than 5% for all cases.

The average single-phase liquid convection heat transfer coefficient over the chip is defined as

$$h_l = \frac{Q_e}{A_s \cdot (T_{chip} - T_{in})} \tag{4}$$

where T_{in} is the coolant temperature at the inlet of the test section and T_{chip} is the average temperature of the upper surface of the chip which is estimated from the measured data for the lower surface of the chip by accounting for the 1-D heat conduction across the chip. The use of the inlet instead of the bulk liquid temperature in defining h_l is due to the heated section of the channel is short when compared with the hydraulic diameter of the channel. On the other hand, the average boiling heat transfer coefficient for the coolant flow over the silicon chip is defined as

$$h_{r,sub} = \frac{Q_e}{A_s \cdot (T_{chip} - T_r)} \tag{5}$$

here T_r is the local mean liquid coolant temperature and is estimated by assuming that it varies linearly in the flow direction. This definition for $h_{r,sub}$ is also used by Kandlikar [20], Bao et al. [21] and Fujita et al. [22].

Uncertainties of the single-phase liquid convection and flow boiling heat transfer coefficients and other parameters are estimated by the procedures proposed by Kline and McClintock [23]. The detailed results from this uncertainty analysis are summarized in Table 1.

4. Results and discussion

The present experiments are conducted for the FC-72 mass flux G varying from 287 kg/m^2 s to 431 kg/m^2 s (inlet liquid FC-72 velocity ranging from 0.18 to 0.27 m/s), the coolant inlet subcooled temperature ΔT_{sub} from 2.3 °C to 4.3 °C, and the imposed heat flux q'' from 0.1 W/cm^2 to 10 W/cm^2. Besides, three silicon chips with the smooth, pin-finned 200 and pin-finned 100 surfaces described previously are tested. The coolant is at a slightly subatmospheric pressure with T_{sat} = 54.3 °C. In the following, selected data will be presented to illustrate the effects of the experimental parameters including the coolant mass flux, imposed heat flux, inlet liquid subcooling and surface micro-structures on the FC-72 subcooled flow boiling heat transfer performance and associated bubble characteristics.

Before conducting the flow boiling experiments, steady single-phase convective heat transfer coefficient is measured for liquid FC-72 flow over the smooth silicon chip. The results are compared with that from Gersey and Mudawar [24]. Good agreement is

Pin-finned 200 surface

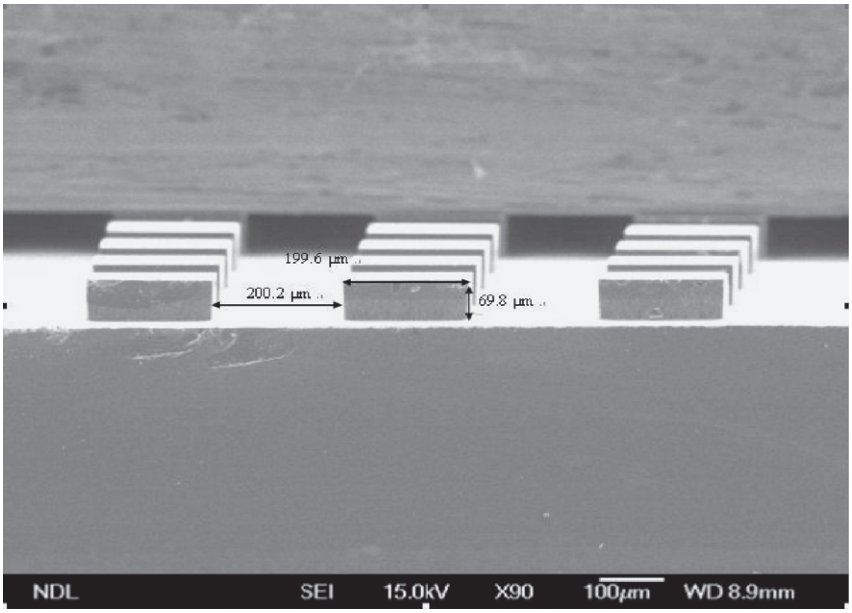

Width × Length × Height: about 200μm × 200μm × 70μm, Space: 200μm

Pin-finned 100 surface

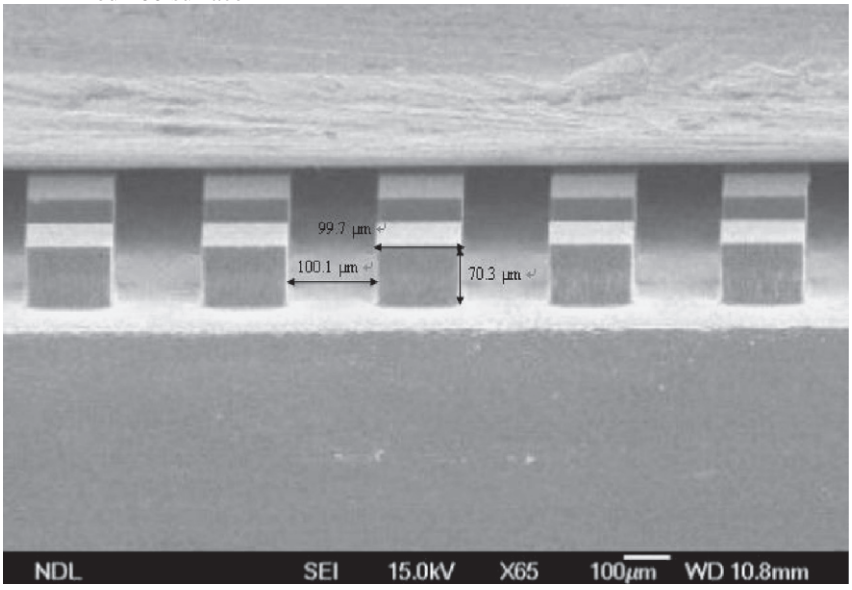

Width × Length × Height: about 100μm × 100μm × 70μm, Space: 100μm

Fig. 3. Photographs of micro-pin-fins on the silicon chip taken by SEM.

noted, as shown in Fig. 4(a). More discussion on the comparison with the single-phase data is given in the previous study [19]. Besides, the liquid convection heat transfer data given in Fig. 4(b) show that adding the micro-pin-fins to the surface can significantly enhance the single-phase convection especially for the smaller fins. The proposed empirical correlation for these data will be given in Section 5.

4.1. Subcooled flow boiling curves

At first, how the experimental parameters affect the boiling curves measured for the FC-72 subcooled flow boiling on the chip surface are presented in Figs. 5 and 6. For a given boiling curve as the imposed heat flux gradually increases from a low value, the temperature of the chip surface increases from a subcooled state to a certain value just exceeding the saturated temperature of the coolant. No bubble nucleation is observed. The heat transfer in this region is completely due to single-phase liquid forced convection. With a continuing increase in the chip surface heat flux, bubbles begin to appear on the surface and there is a sudden drop in the chip surface temperature. We have onset of nucleate boiling (ONB) in the flow. The reason causing the sudden drop in the chip surface temperature at ONB is due to a significant enhancement in the surface heat transfer by the appearance of the boiling on the

Table 1
Summary of the uncertainty analysis.

Parameter	Uncertainty
Rectangular channel geometry	
Length, width and thickness (%)	±0.5%
Area (%)	±1.0%
Parameter measurement	
Temperature, T (°C)	±0.2
Temperature difference, ΔT (°C)	±0.3
System pressure, P (kPa)	±2
Mass flux of coolant, G (%)	±2
Single-phase heat transfer in rectangular channel	
Imposed heat flux, q'' (%)	±4.2
Heat transfer coefficient, h_l (%)	±12.3
Subcooled flow boiling heat transfer in rectangular channel	
Imposed heat flux, q'' (%)	±4.2
Heat transfer coefficient, h_r (%)	±12.3

surface. A close inspection of the data for the single-phase region further reveals that at a higher mass flux of 431 kg/m^2 s the chip surface temperature is somewhat lower for the same imposed heat flux. This obviously results from the increase in h_l with G. Note that except for the imposed heat flux slightly beyond that for ONB the coolant mass flux exhibits little effects on the boiling curves, suggesting the dominance of the surface heat transfer by the fully developed nucleate boiling. Similar results were found by Willingham and Mudawar [2]. However at a higher G the wall superheat and heat flux at ONB are substantially higher. This can be attributed to the fact that at a higher G more energy is needed for the vapor to nucleate from the cavities in the wall since the residence time of the coolant on the chip is shorter. Checking the results in Figs. 5 and 6 discloses that for the pin-finned surfaces the boiling curves show similar trend to that for the smooth surface. A scrutiny of these data further suggests that for the pin-finned surfaces the fully developed nucleate boiling also prevails in the flow after ONB.

Comparing the data in Figs. 5 and 6 for different inlet liquid subcoolings for the chip with a smooth surface indicates that the wall superheat and the imposed heat flux for the incipient boiling are both somewhat higher at a higher ΔT_{sub}. Besides, at the same ΔT_{sat} but at a higher ΔT_{sub} the boiling heat flux is noticeably higher only in the region just beyond ONB. Elsewhere in the fully developed nucleate boiling region the effects of the inlet liquid subcooling are insignificant. This is in accordance with the results from Heindel et al. [3] and Tso et al. [4]. It is of interest to note that the delay of the onset of nucleate boiling heat flux to a higher value at increasing inlet liquid subcooling results from the fact that more energy is needed for boiling inception on the chip surface when the bulk liquid is in a more subcooled state. For the finned surface, the effects of ΔT_{sub} on the wall superheat and wall heat flux at the incipient boiling are similar to the chip with the smooth surface. Moreover, for the finned surface the surface heat flux is slightly higher in the single-phase region for a higher ΔT_{sub}.

Examining the results in Figs. 5 and 6 for different chip surface micro-structures for the FC-72 subcooled flow boiling clearly shows that in both the single-phase and nucleate boiling regions at the same wall superheat the chip surface heat flux is highest for the pin-finned 100 surface and lowest for the smooth surface. This indicates that using the micro-pin-finned structure can effectively enhance the single-phase and subcooled flow boiling heat transfer from the chip. The large increase in the total surface area by the micro-pin-fins is indeed beneficial also for the subcooled flow boiling heat transfer. Note that the boiling curves for the pin-finned 100 surface are relatively steep in the nucleate boiling region, implying very effective heat removal by the bubble nucleation in this region. Besides, the wall superheat required for the boiling inception is substantially lower for the pin-finned 100 surface. This is ascribed to the increase in the density of the active nucleation sites by the surface micro-structures. Particularly, in the corner region of the pin-fins the bubbles are found to appear at a lower ΔT_{sat} .

A similar study conducted recently by Ma et al. [25] for a chip surface with micro-pin-fins of much smaller cross sections shows that the subcooled flow boiling heat transfer over the much smaller pin-fins is substantially better when compared with the present data. However, the surface temperature undershoot at ONB is not seen in their study.

4.2. Subcooled flow boiling heat transfer coefficients

Next, we examine how the subcooled flow boiling heat transfer coefficient $h_{r,sub}$ is affected by the experimental parameters. The results presented in Fig. 7 for the variations of $h_{r,sub}$ with the imposed heat flux reveal that for the three tested surfaces the coolant mass flux exhibits relatively small influences on $h_{r,sub}$. However, for a given coolant mass flux the boiling heat transfer coefficient increases substantially with the imposed heat flux. Besides, the inlet subcooling of the coolant also shows a significant effect on the boiling heat transfer coefficient. Specifically, $h_{r,sub}$ is higher for a lower ΔT_{sub}. Moreover, the inlet subcooling effect is stronger at a higher imposed heat flux. Finally, it is also noted from Fig. 7 that in the FC-72 subcooled flow boiling the surface micro-structures in the form of micro-pin-fins produce some positive effects on the boiling heat transfer coefficient at high imposed heat flux. This results from the fact that upon adding the pin-fin structures to the chip surface, the increase in the active nucleation sites on the surface effectively promotes the boiling heat transfer performance. Besides, the heat transfer is further enhanced by a serpentine motion of subcooled liquid between adjacent rows of pin-fins, which in turn augments turbulent mixing. Furthermore, development of multiple thermal entry regions at the top surfaces of individual pin-fins exists.

4.3. Bubble characteristics

To elucidate the subcooled flow boiling heat transfer characteristics, the bubble characteristics obtained from the present flow visualization are examined in the following. At first, the top views of the boiling flow for various experimental parameters are shown in Figs. 8 and 9 for the tested chips. As the chip surface temperature exceeds the boiling incipience superheat, tiny bubbles are observed on the active nucleation sites and they grow rapidly but still attach to the chip surface. These bubbles then detach and slide along the heating surface. At low imposed heat flux, the bubble growth and departure processes are found to be nearly regular and the bubbles are nearly spherical. At a higher imposed heat flux, a lower coolant mass flux, and a lower inlet liquid subcooling, more nucleation sites are activated and more bubbles depart from the chip. Besides, more bubbles are seen on the pin-finned 100 surface. Thus at these conditions merging of small bubbles to form large bubbles occurs more frequently.

To quantify the bubble characteristics, the measured data for the mean bubble departure diameter, bubble departure frequency and active nucleation site density are illustrated in Figs. 10–12 for various experimental parameters. The results in Fig. 10 manifest that increasing the coolant mass flux can significantly reduce the size of the bubbles departing from the chip surfaces for the wide range of q'' tested here and for different degrees of ΔT_{sub}. This is simply due to the higher drag acting on the bubbles still attaching to the cavities by the surrounding subcooled liquid flowing at a higher speed for a higher G. It is also noted that at the higher inlet liquid subcooling the bubbles departing from the heated surface

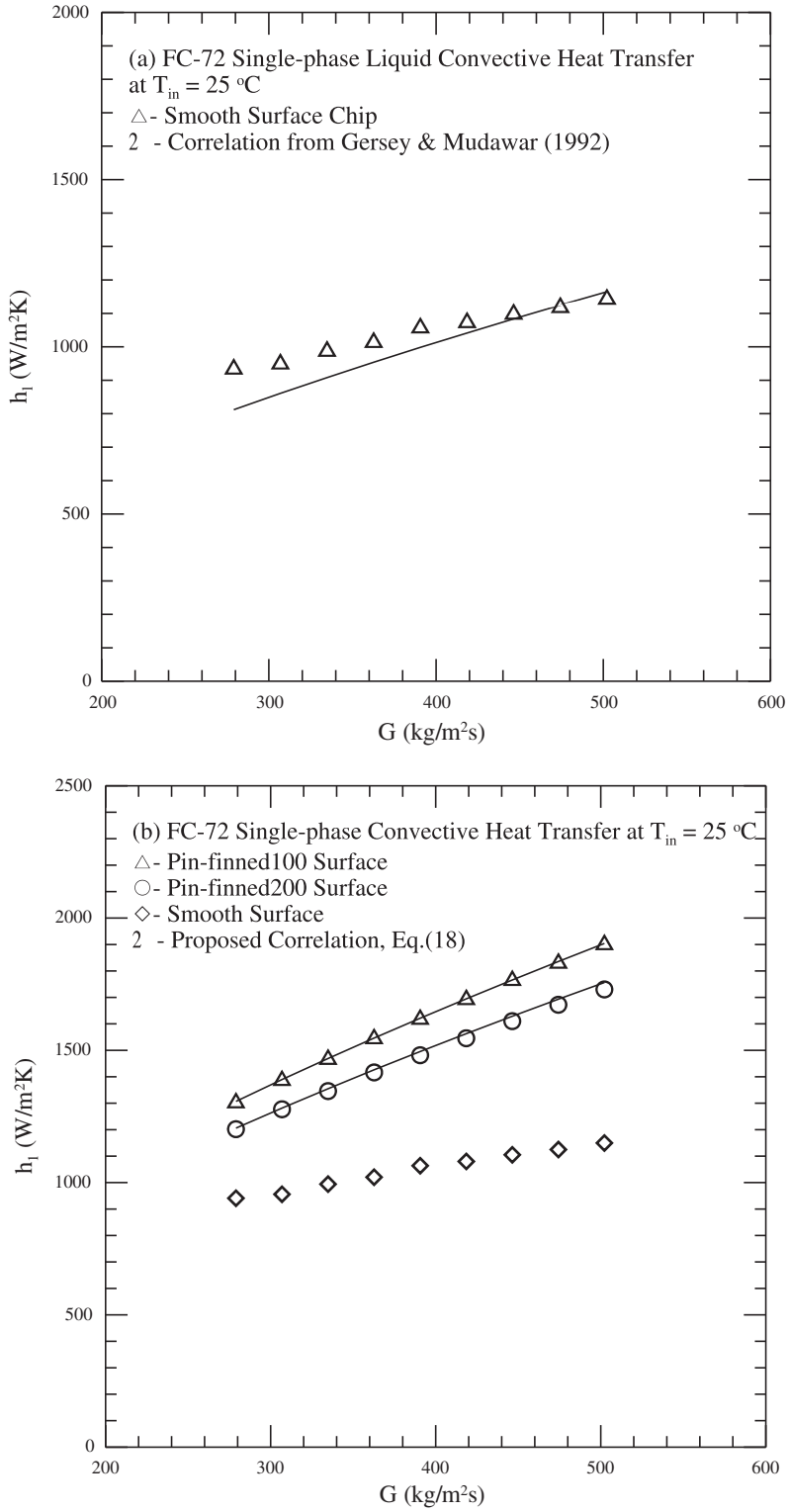

Fig. 4. Comparison of the present single-phase liquid convection heat transfer coefficient for the chip with (a) a smooth surface with the correlation of Gersey and Mudawar [24] and (b) micro-pin-fins with the proposed correlation.

are smaller. This is considered to result from the stronger vapor condensation inside the bubbles for a higher ΔT_{sub}. It is further noted from Fig. 10 that the presence of the micro-pin-fins on the chips causes a significantly earlier departure of the bubbles from the chip surface. This is because the liquid coolant may be partially accelerated when it flows through the space between the adjacent pin-fins. The partially accelerated coolant can effectively enhance the drag force acting on the bubbles and causes them to detach earlier from the finned surface. Note that the mean bubble departure diameter is smallest for the surface with larger fins. This is attributed to the fact that for the pin-finned 100 surface although the partial coolant acceleration is more pronounced, the space between the adjacent fins are so small and the bubbles already contact the sides of the fins before departure. Therefore, the bubbles

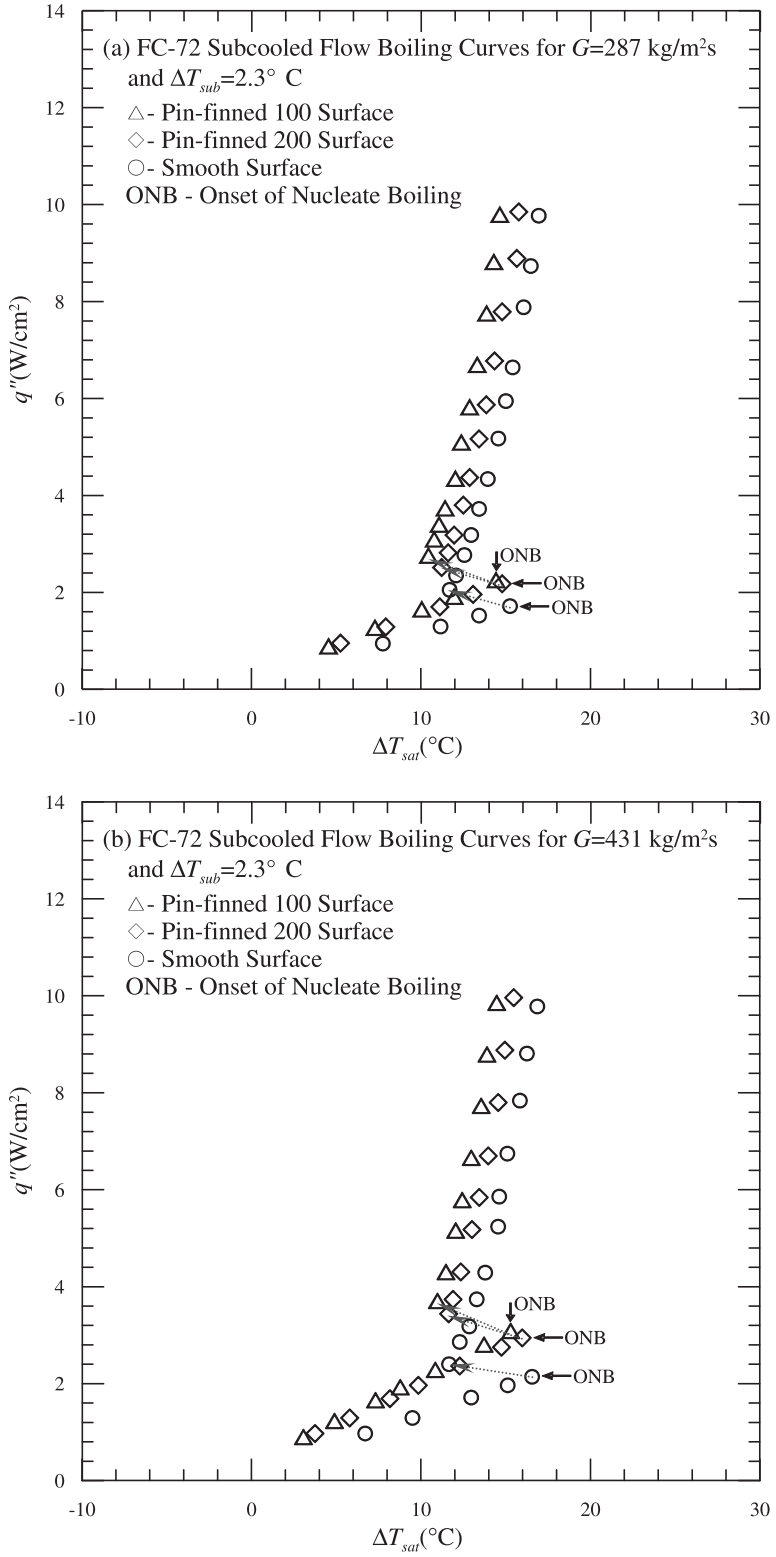

Fig. 5. Boiling curves affected by surface micro-structures for ΔT_{sub} = 2.3 °C at (a) G = 287 kg/m^2 s ($u_{l,in}$ = 0.18 m/s) and (b) G = 431 kg/m^2 s ($u_{l,in}$ = 0.27 m/s).

grow for a longer period of time before they detach from the chip surface. Longer bubble growth time causes the growing bubble to keep absorbing energy from the heated surface and results in a larger mean bubble departure diameter. It is worth mentioning that the mean bubble departure diameter on the pin-finned 100 surface is still smaller than that on the smooth surface. This is conjectured to be due to that for the pin-finned 100 surface the fin height is smaller than the mean bubble departure diameter so the partial coolant acceleration effect still plays an important role in affecting the bubble departure processes.

Then, the data given in Fig. 11 manifest that in the FC-72 subcooled flow boiling the mean bubble departure frequency can be substantially augmented by raising the coolant mass flux. The mass flux effects are slightly stronger at a higher imposed heat

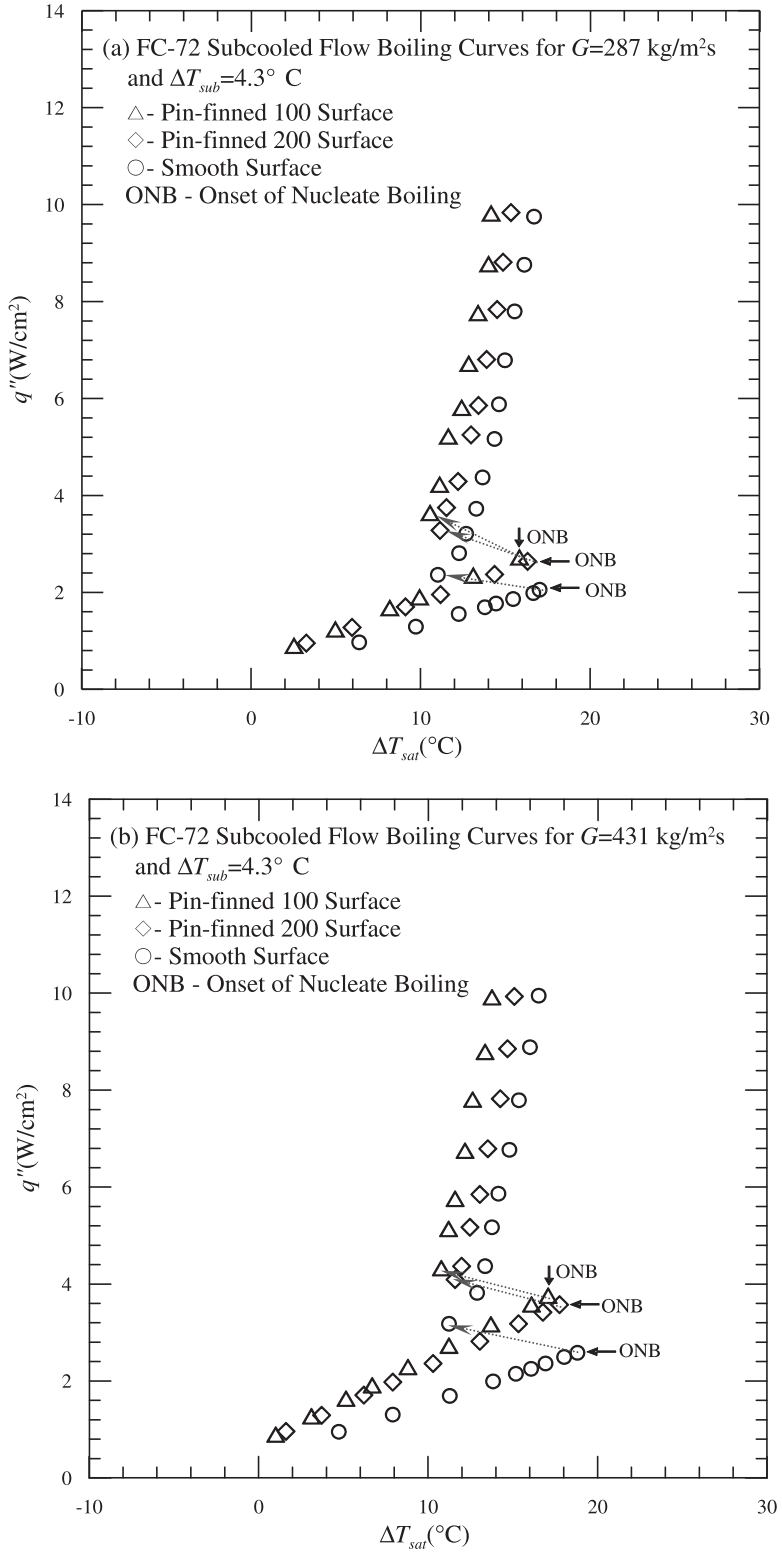

Fig. 6. Boiling curves affected by surface micro-structures for ΔT_{sub} = 4.3 °C at (a) G = 287 kg/m^2 s ($u_{l,in}$ = 0.18 m/s) and (b) G = 431 kg/m^2 s ($u_{l,in}$ = 0.27 m/s).

flux. The increase of f with G is attributed again to the higher drag on the bubbles still attaching to the chip surface by the subcooled liquid coolant moving at a higher speed for a higher G. This, in turn, causes an earlier departure of the bubbles from the surface, resulting in a higher departure frequency. It is also noted that the mean bubble departure frequency increases noticeably with the imposed heat flux. Moreover, the bubble departure frequency is somewhat higher for a lower inlet liquid subcooling, which is also observed by Yin et al. [8] for the subcooled flow boiling of R-134a in an annular duct. This again results from the fact that the vapor condensation in the bubble is less important and the bubble growth rate is faster for a lower ΔT_{sub}. Note that the effects of ΔT_{sub} on f are more pronounced for a higher coolant mass flux. Finally, the data given in Fig. 11 also indicate that the bubble departure fre-

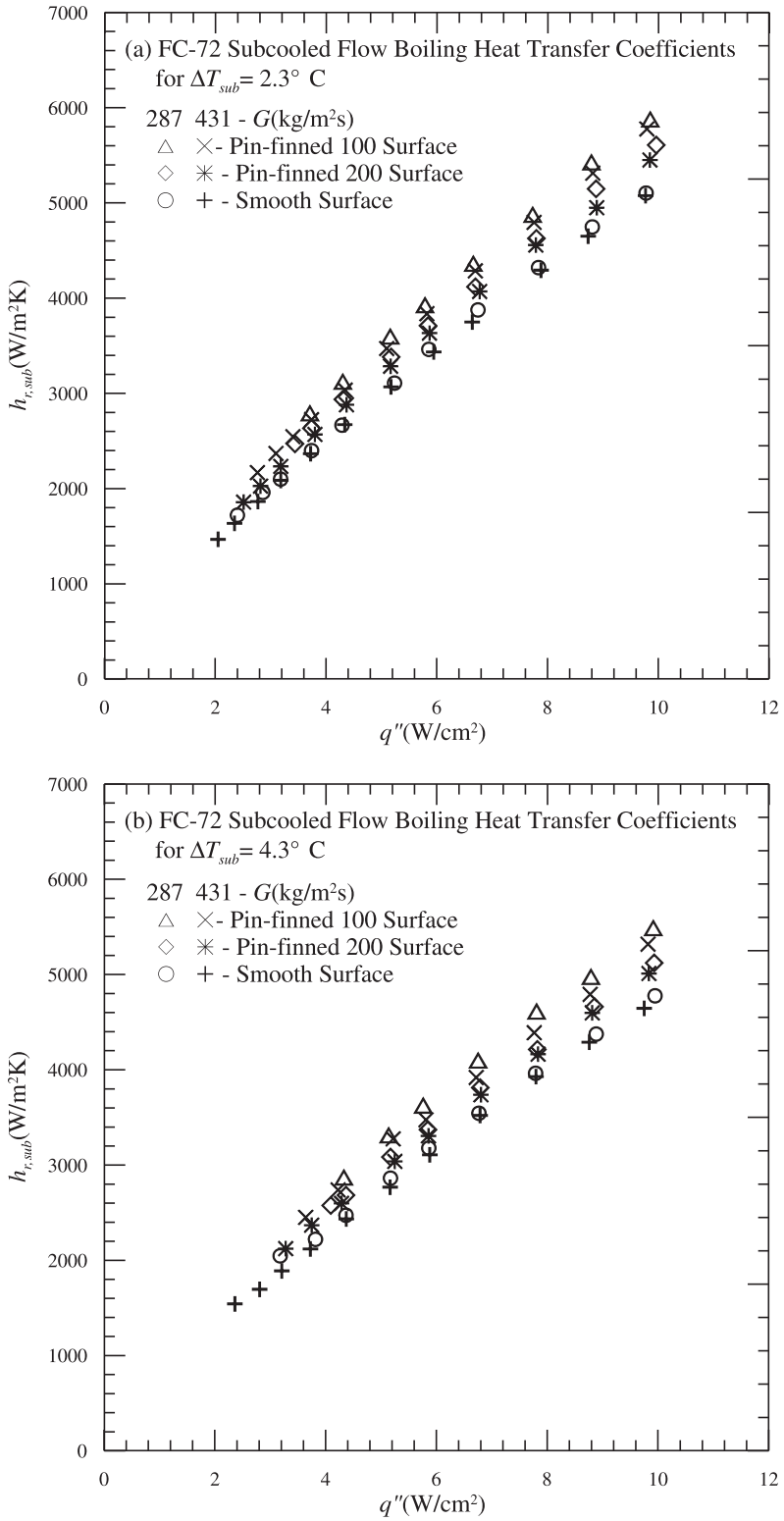

Fig. 7. Subcooled flow boiling heat transfer coefficients affected by surface micro-structures for (a)ΔT_{sub} = 2.3 °C and (b)ΔT_{sub} = 4.3 °C.

quency can be enhanced significantly by using the pin-finned 200 surface. For the pin-finned 100 surface the space between the adjacent fins is too small, leading to a delay in the departure of bubbles.

Finally, attention is turned to the data for the mean active nucleation site density N_{ac} shown in Fig. 12. N_{ac} is calculated based on the surface area of a bare chip. An increase in the coolant mass flux results in somewhat lower N_{ac} for the three surfaces. This relates directly to the higher imposed heat flux is needed for the boiling inception at a higher G, as already discussed in the previous section. Comparing the results in Fig. 12(a) and (b) reveals that the effects of the inlet liquid subcooling on N_{ac} are rather slight. Finally, adding the micro-pin-fins to the chip surface can effectively

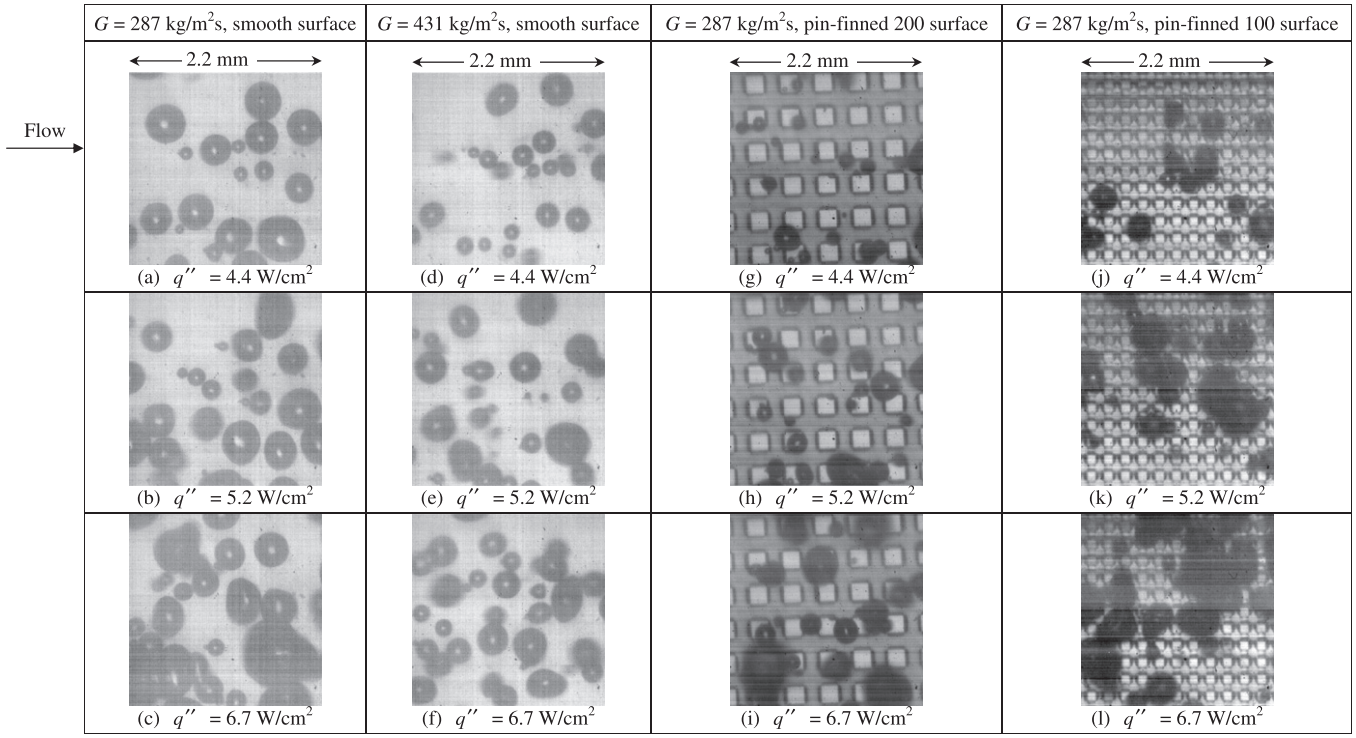

Fig. 8. Photos of bubbles in the subcooled flow boiling of FC-72 for various imposed heat fluxes, mass fluxes and chip surfaces at ΔT_{sub} = 2.3 °C.

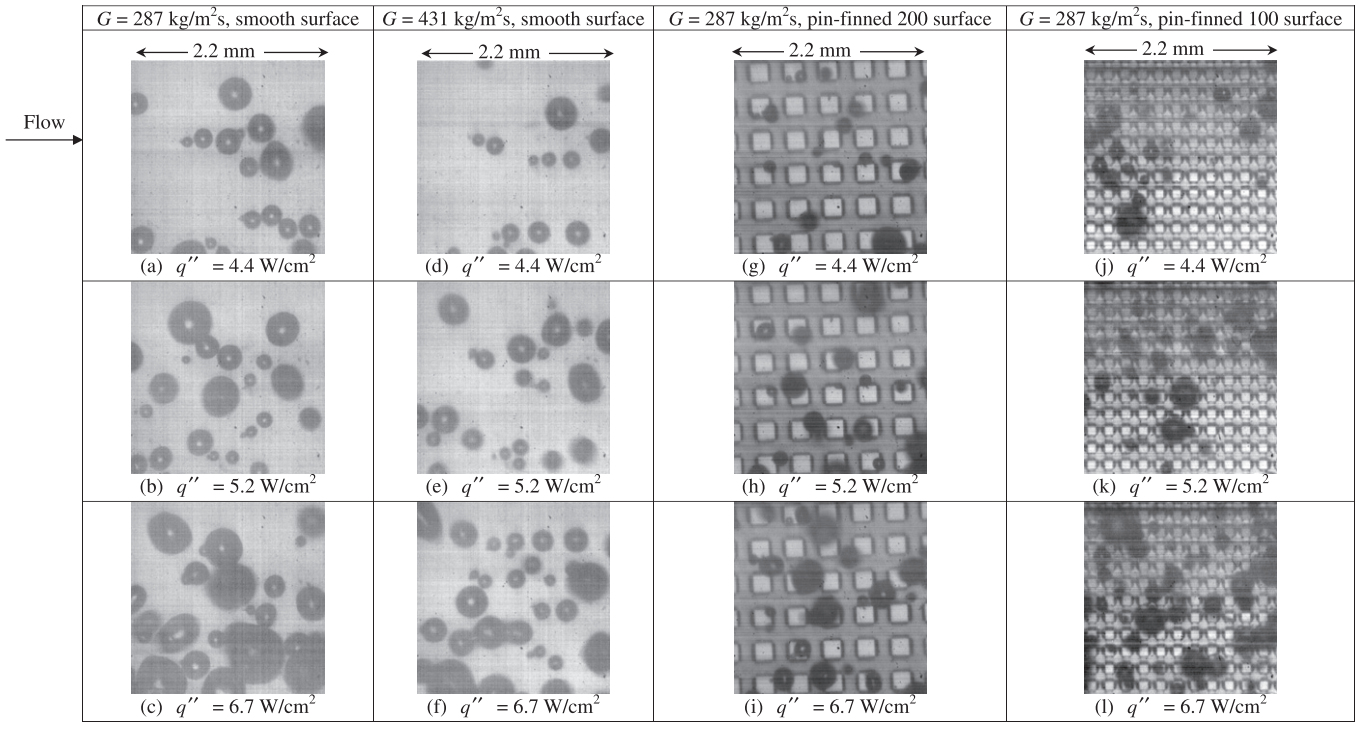

Fig. 9. Photos of bubbles in the subcooled flow boiling of FC-72 for various imposed heat fluxes, mass fluxes and chip surfaces at ΔT_{sub} = 4.3 °C.

increase the active nucleation sites. This is ascribed to the increase in the surface area of micro-pin-fins. More specifically, the nucleation site density on the pin-finned 100 surface is higher than that on the pin-finned 200 surface.

5. Correlation equations

To facilitate thermal design for electronics cooling, empirical correlations based on the present data for the bubble characteris-

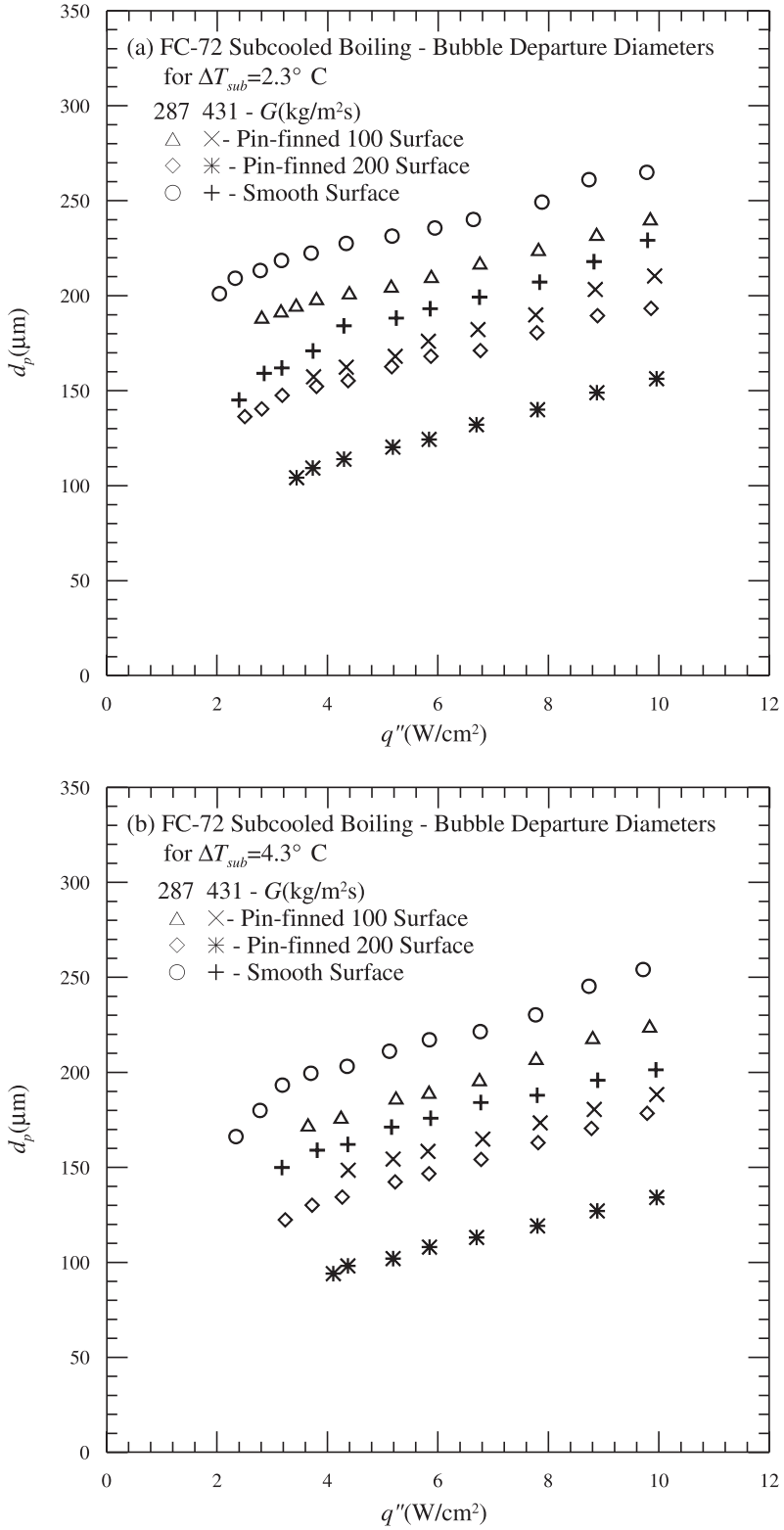

Fig. 10. Mean bubble departure diameters for subcooled flow boiling affected by surface micro-structures for (a) ΔT_{sub} = 2.3 °C and (b) ΔT_{sub} = 4.3 °C.

tics and heat transfer coefficient in the subcooled flow boiling of FC-72 on the heated silicon chip flush-mounted on the bottom of the rectangular channel are proposed.

First, empirical correlations for the average bubble departure diameter are proposed as

$$\bar{d}_p \equiv \frac{d_p}{\sqrt{\sigma/(g\cdot\Delta\rho)}} = \frac{0.38\cdot(\rho_l/\rho_v)^{1.32}}{\mathrm{Re}_l^{0.2}\cdot\left[Ja' + \frac{0.6\cdot(\rho_l/\rho_v)^{0.9}}{\mathrm{Bo}^{0.3}\mathrm{Re}_l^{0.1}}\right]} \quad \text{for smooth surface} \tag{6}$$

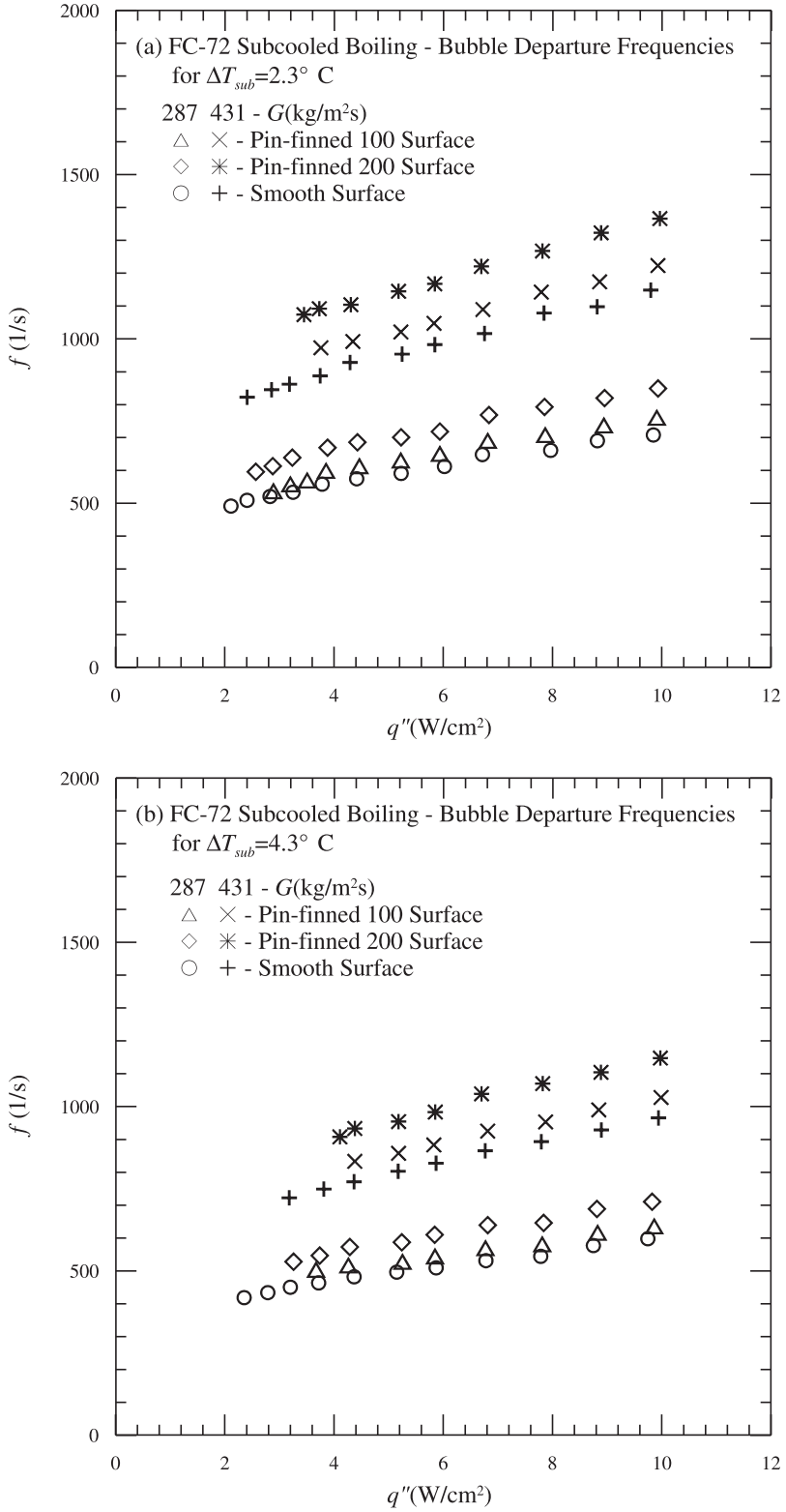

Fig. 11. Mean bubble departure frequencies for subcooled flow boiling affected by surface micro-structures for (a) ΔT_{sub} = 2.3 °C and (b)ΔT_{sub} = 4.3 °C.

and

$$\bar{d}_p \equiv \frac{d_p}{\sqrt{\sigma/(g\cdot\Delta\rho)}} = \frac{0.17\cdot(\rho_l/\rho_v)^{1.32}\cdot F_{d,sub}}{\mathrm{Re}_l^{0.2}\cdot\left[Ja' + \frac{0.6\cdot(\rho_l/\rho_v)^{0.9}}{\mathrm{Bo}^{0.3}\mathrm{Re}_l^{0.1}}\right]} \quad \text{for pin-finned surfaces} \tag{7}$$

with the fin-geometry factor $F_{d,sub}$ included here to account for the geometrical arrangement of the micro-pin-fins which is correlated as

$$F_{d,sub} = \left(\frac{S_f}{H}\right)^{-0.125}\left(\frac{H-B_f}{W_f}\right)^{0.05}\left(\frac{N\cdot A_f}{A_s}\right)^{0.4} \tag{8}$$

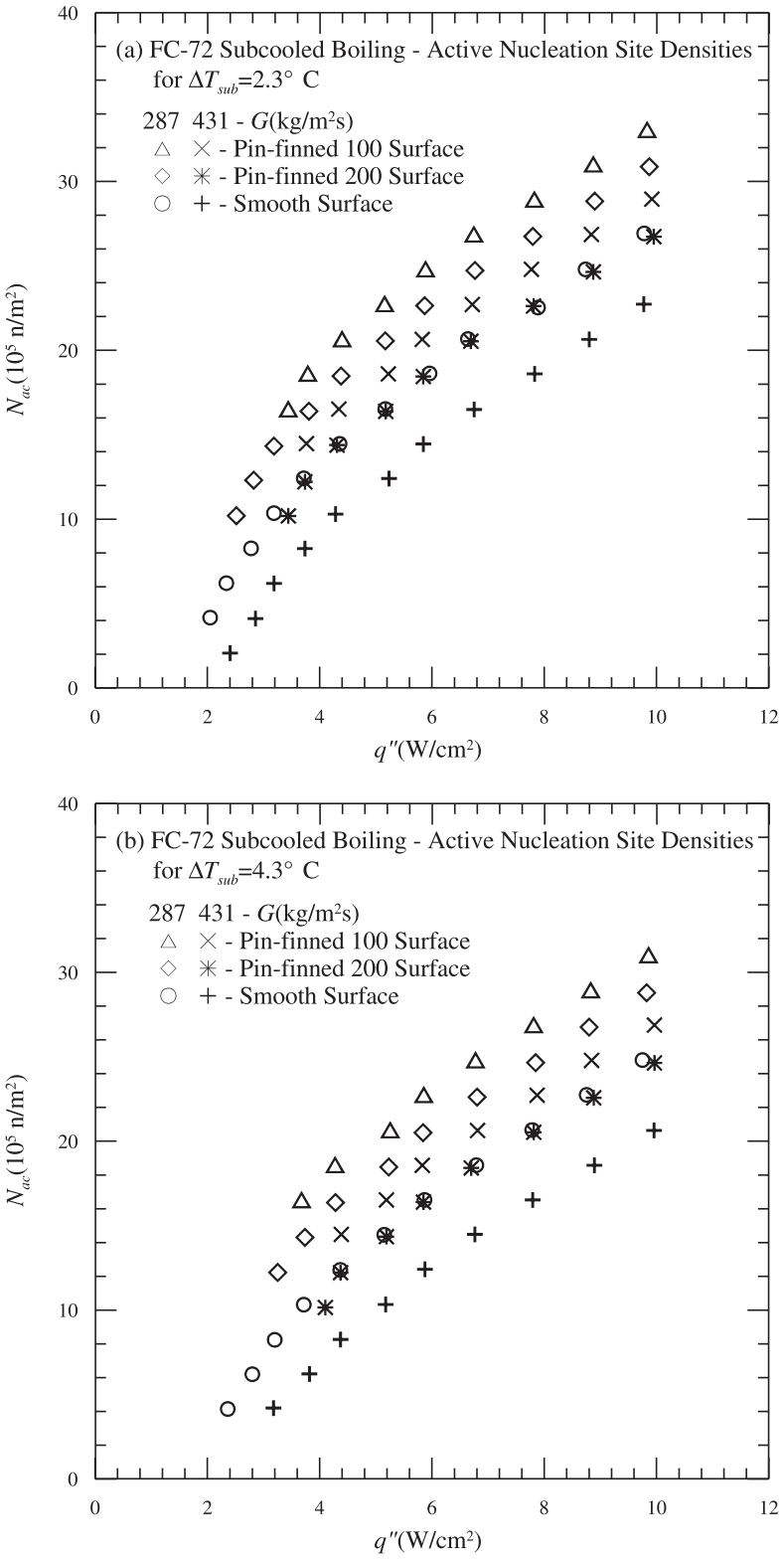

Fig. 12. Mean active nucleation site densities for subcooled flow boiling affected by surface micro-structures for (a) ΔT_{sub} = 2.3 °C and (b) ΔT_{sub} = 4.3 °C.

Here Bo, Ja and Re_l are respectively the Boiling, Jacob and liquid Reynolds numbers. Fig. 13(a) shows that the present experimental data fall within ± 20% of the above correlations.

Next, empirical equations are provided to correlate the data for the mean bubble departure frequency as

$$\bar{f} \equiv \frac{f \cdot d_p}{\mu_l/(\rho_l \cdot D_h)} = 0.57 \mathrm{Re}_l^{1.4} \cdot \mathrm{Ja}'^{-0.3} \cdot \mathrm{Bo}^{0.5} \quad \text{for smooth surface} \tag{9}$$

and

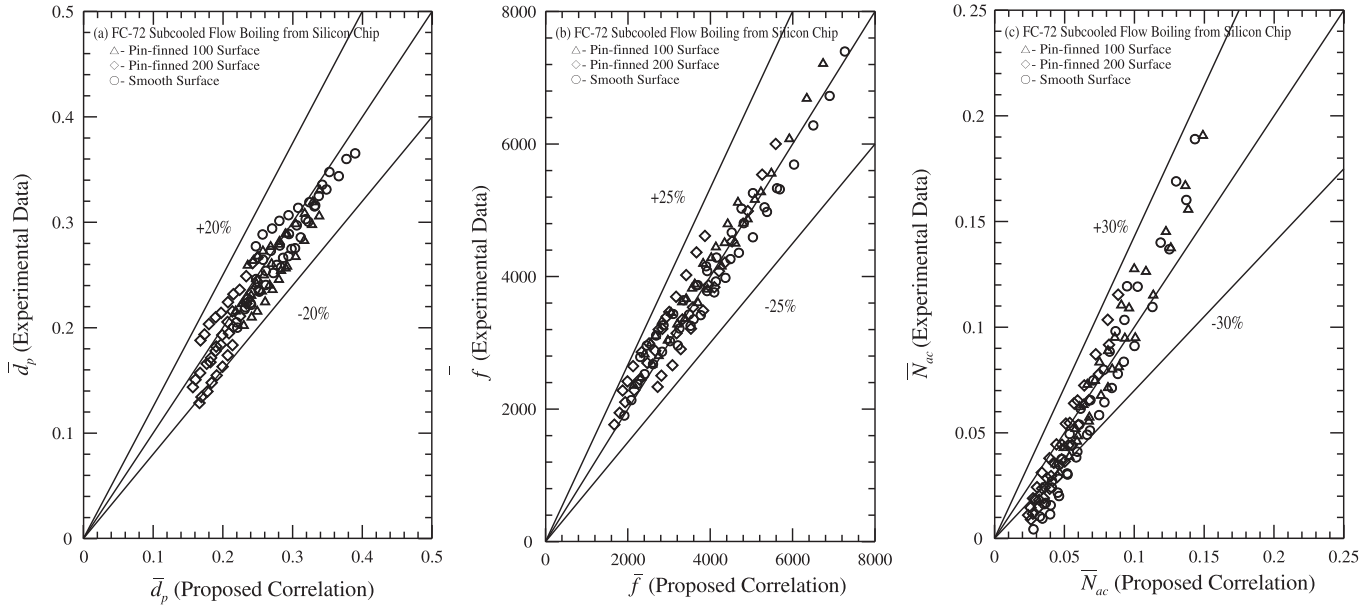

Fig. 13. Comparison of the measured data with the proposed correlations in the subcooled flow boiling of FC-72 for (a) mean bubble departure diameter, (b) mean bubble departure frequency and (c) mean active nucleation site density.

$$\bar{f} \equiv \frac{f \cdot d_p}{\mu_l/(\rho_l \cdot D_h)} = 0.175\mathrm{Re}_l^{1.42} \cdot \mathrm{Ja}'^{-0.3} \cdot \mathrm{Bo}^{0.53} \cdot F_{f,sub} \quad \text{for pin-finned surfaces} \tag{10}$$

with the fin-geometry factor $F_{f,sub}$ correlated as

$$F_{f,sub} = \left(\frac{S_f}{H}\right)^{0.12}\left(\frac{H-B_f}{W_f}\right)^{0.4}\left(\frac{N\cdot A_f}{A_s}\right)^{-0.02} \tag{11}$$

Fig. 13(b) indicates that the present experimental data for $\bar{f}$ can be correlated with the deviation less than ± 25% by Eqs. (9) and (10).

Moreover, empirical correlations for the mean active nucleation site density in the FC-72 subcooled flow boiling deduced from the present flow visualization are proposed as

$$\overline{N}_{ac} \equiv N_{ac} \cdot d_p^2 = 65 \cdot \mathrm{Bo}^{0.87} \cdot \mathrm{Re}_l^{-0.15} \cdot \mathrm{Ja}'^{-0.05} \quad \text{for smooth surface} \tag{12}$$

and

$$\overline{N}_{ac} \equiv N_{ac} \cdot d_p^2 = 48 \cdot \mathrm{Bo}^{0.85} \cdot \mathrm{Re}_l^{-0.15} \cdot \mathrm{Ja}'^{-0.1} \cdot F_{n,sub} \quad \text{for pin-finned surfaces} \tag{13}$$

with the geometry factor $F_{n,sub}$ correlated as

$$F_{n,sub} = \left(\frac{S_f}{H}\right)^{-0.15}\left(\frac{H-B_f}{W_f}\right)^{-0.06}\left(\frac{N\cdot A_f}{A_s}\right) \tag{14}$$

The comparison in Fig. 13(c) shows that more than 80% of the present experimental data fall within ± 30% of the correlations given in Eqs. (12) and (13).

Finally, the total heat flux input from the chip surface to the boiling flow q_t'' is considered to be roughly composed of two parts: one resulting from the bubble nucleation q_b'' and another due to the single-phase liquid forced convection q_c'' [19]. Thus

$$q_t'' = q_b'' + q_c'' \tag{15}$$

Here q_b'' and q_c'' can be individually calculated from the quantitative data for the bubble characteristics as

$$q_b'' = \rho_v \cdot V_v \cdot f \cdot N_{ac} \cdot i_{lv} \tag{16}$$

Besides, q_c'' can be estimated from the single-phase liquid convection as

$$q_c'' = E \cdot h_l \cdot \Delta T_{sat} \tag{17}$$

where E is an enhancement factor added to account for the agitating motion of the bubbles which can enhance the single-phase liquid convection heat transfer. The heat transfer coefficient h_l is estimated from the empirical correlation for Nu_l proposed by Lie et al. [19] as

$$\mathrm{Nu}_l = 0.33 \cdot \mathrm{Re}_l^{0.64} \cdot \mathrm{Pr}^{1/3} \cdot F_{sp} \tag{18}$$

where F_{sp} is a factor to account for the geometry effect of the square pin-finned surface on the liquid convection heat transfer and it was correlated in [19] as

$$F_{sp} = \left(\frac{S_f}{H}\right)^{-0.15}\left(\frac{H-B_f}{W_f}\right)^{-0.06}\left(\frac{N\cdot A_f}{A_s}\right)^{0.04} \tag{19}$$

From the experimental data, the enhancement factor E can be empirically correlated as

$$E = 5.5 \cdot N_{conf}^{0.5} \cdot Fr_l^{0.2} \cdot (1 + 275 \cdot Bo)^{1.8} \quad \text{for smooth surface} \tag{20}$$

and

$$E = 3.3 \cdot N_{conf}^{0.5} \cdot Fr_l^{0.2} \cdot (1 + 250 \cdot Bo)^{1.8} \cdot F_{E,sub} \quad \text{for pin-finned surfaces} \tag{21}$$

with the fin-geometry factor $F_{E,sub}$ correlated as

$$F_{E,sub} = \left(\frac{S_f}{H}\right)^{-0.16}\left(\frac{H-B_f}{W_f}\right)^{-0.07}\left(\frac{N\cdot A_f}{A_s}\right)^{0.04} \tag{22}$$

The comparison shown in Fig. 14 indicates that the present boiling heat transfer data can be correlated with the deviation less than ±25% by the above empirical correlation.

To further improve our understanding of the boiling heat transfer mechanisms, the relative importance of the latent heat transfer associated with the bubble nucleation and the sensible heat transfer due to the single-phase liquid convection needs to be examined. This is presented in Fig. 15 by showing the data for q_b/q_t, which is

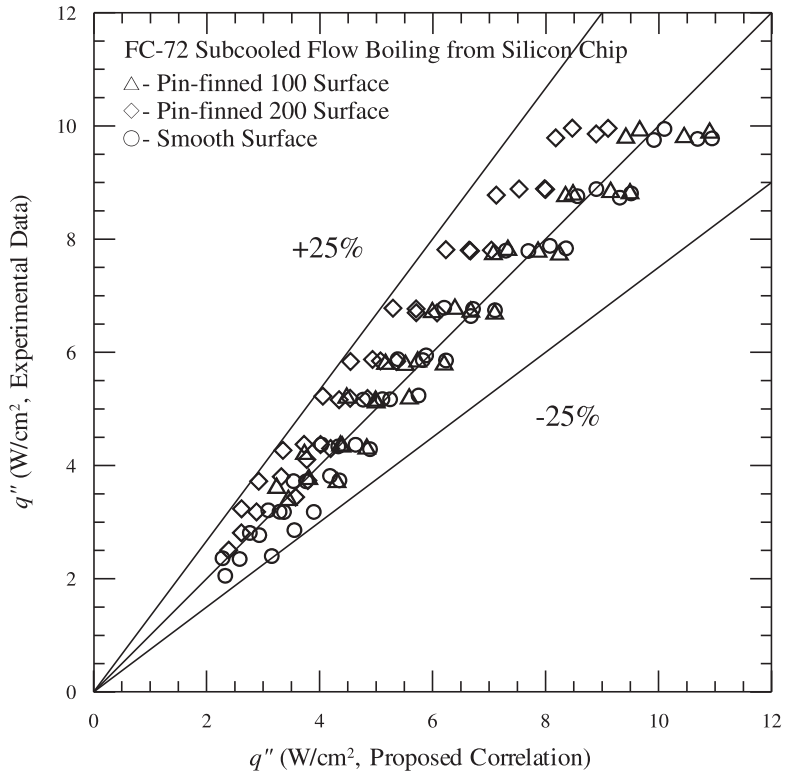

Fig. 14. Comparison of the measured heat transfer data with the proposed correlation in the subcooled flow boiling of FC-72.

estimated by Eqs. (15)–(22), for ΔT_{sub} = 2.3 °C for the three tested surface. The results clearly indicate that the latent heat transfer becomes increasingly important for a higher imposed heat flux and a lower coolant mass flux, which is more pronounced for the smooth and pin-finned 100 surfaces. Besides, the latent heat transfer still accounts for a small fraction of the total heat transfer. This is a direct consequence of the low imposed heat flux ($\leqslant$10 W/cm^2) covered in the present study. It is of interest to note from the data that at a higher inlet liquid subcooling the latent heat transfer is even less important.

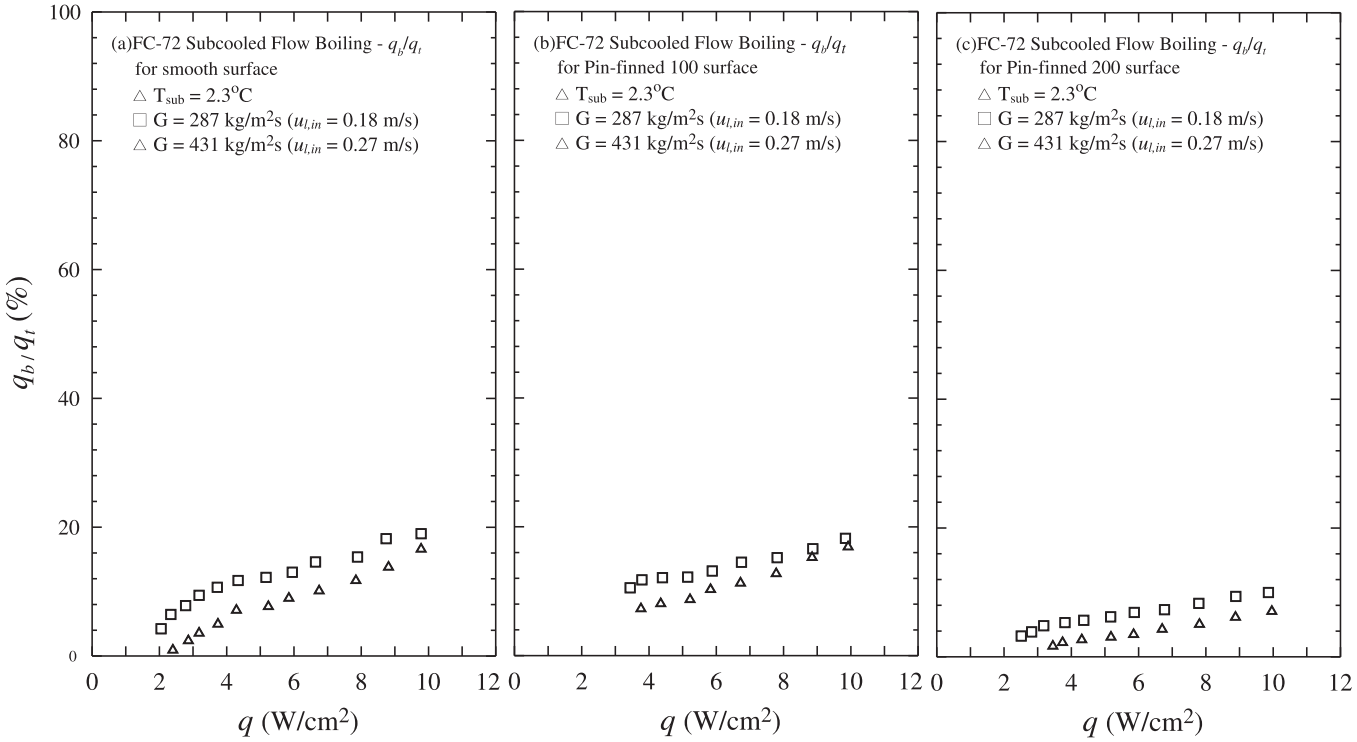

Fig. 15. Variations of q_b/q_t with the imposed heat flux for (a) smooth surface, (b) pin-finned 100 surface and (c) pin-finned 200 surface at ΔT_{sub} = 2.3 °C.

6. Concluding remarks

Subcooled flow boiling heat transfer and associated bubble characteristics of FC-72 over a heated micro-pin-finned silicon chip flush-mounted onto the bottom of a rectangular channel have been investigated experimentally. The effects of the coolant mass flux, inlet liquid subcooling, and surface micro-structures of the chip on the measured data have been examined in detail. Furthermore, empirical equations to correlate the data are proposed to facilitate thermal design for electronics cooling by flow boiling. Major results obtained here can be summarized as follows:

(1) Increases in the coolant mass flux and inlet liquid subcooling delay the boiling incipience to a higher surface heat flux. The temperature of the chip surface is lowered significantly by increasing the coolant mass flux and inlet liquid subcooling in the single-phase region, but it is only slightly affected in the nucleate boiling region. Besides, adding the micro-pin-fins to the chips can effectively lower the temperature of chip surface in both single-phase and two-phase regions.
(2) The coolant mass flux shows little influence on the subcooled flow boiling heat transfer coefficient. An increase in the inlet liquid subcooling, however, results in a slight reduction in the subcooled flow boiling heat transfer coefficient. Besides, the boiling heat transfer coefficient increases substantially with the imposed heat flux. Furthermore, adding the micro-pin-fins to the chip is beneficial in enhancing the single-phase and two-phase heat transfer.
(3) Mean bubble departure diameter is reduced at increasing coolant mass flux and inlet liquid subcooling. Besides, the higher imposed heat flux results in a larger bubble departure diameter but smaller mean bubble departure diameter is found on the pin-finned surfaces.
(4) Bubble departure frequency increases with the coolant mass flux and imposed heat flux. However, at a higher inlet liquid subcooling the bubble departure frequency is lower. On the other hand, higher bubble departure frequency is noted on the pin-finned surfaces.
(5) Active nucleation site density is less for higher coolant mass flux and inlet liquid subcooling. However, the opposite is the case for a higher imposed heat flux and for the chip with the micro-pin-fin structures.
(6) The results presented here suggest that adding a microstructure in the form of micro-pin-fins to a chip surface can effectively augment the subcooled flow boiling heat transfer over the surface and can be considered for the cooling of electronic devices with a high power dissipation. Besides, a more detailed study is needed to find the optimal arrangement of the pin-fins for the flow boiling of FC-72 over the chip.

Acknowledgement

The financial support of this study by the engineering division of National Science Council of Taiwan, ROC through the Contract NSC 96-2221-E-009-133-MY3 is greatly appreciated.

References

[1] R.E. Simons, Thermal management of electronic packages, Solid State Technol. (1983) 131–137.
[2] T.C. Willingham, I. Mudawar, Forced-convection boiling and critical heat flux from a linear array of discrete heat sources, Int. J. Heat Mass Transfer 35 (1992) 2879–2890.
[3] T.J. Heindel, S. Ramadhyani, F.P. Incropera, Liquid immersion cooling of a longitudinal array of discrete heat sources in protruding substrates: II – Forced convection boiling, ASME J. Electron. Packag. 114 (1992) 63–70.
[4] C.P. Tso, K.W. Tou, G.P. Xu, Flow boiling critical heat flux of FC-72 from flush-mounted and protruded simulated chips in a vertical rectangular channel, Int. J. Multiphase Flow 26 (2000) 351–365.
[5] K.R. Samant, T.W. Simon, Heat transfer from a small heated region to R-113 and FC-72, ASME J. Heat Transfer 111 (1989) 1053–1059.
[6] Y. Ma, J.N. Chung, A study of bubble dynamics in reduced gravity forced-convection boiling, Int. J. Heat Mass Transfer 44 (2001) 399–415.
[7] R. Situ, Y. Mi, M. Ishii, M. Mori, Photographic study of bubble behavior in forced convection subcooled boiling, Int. J. Heat Mass Transfer 47 (2004) 3659–3667.
[8] C.P. Yin, Y.Y. Yan, T.F. Lin, B.C. Yang, Subcooled flow boiling heat transfer of R-134a and bubble characteristics in a horizontal annular duct, Int. J. Heat Mass Transfer 43 (2000) 1885–1896.
[9] S.H. Chang, I.C. Bang, Won-Pil Baek, A photographic study on the near-wall bubble behavior in subcooled flow boiling, Int. J. Therm. Sci. 41 (2002) 609–618.
[10] I.C. Bang, S.H. Chang, Won-Pil Baek, Visualization of the subcooled flow boiling of R-134a in a vertical rectangular channel with an electrically heated wall, Int. J. Heat Mass Transfer 47 (2004) 4349–4363.
[11] R. Maurus, V. Ilchenko, T. Sattelmayer, Study of the bubble characteristics and the local void fraction in subcooled flow boiling using digital imaging and analyzing techniques, Exp. Therm. Fluid Sci. 26 (2002) 147–155.
[12] R. Maurus, V. Ilchenko, T. Sattelmayer, Automated high-speed video analysis of the bubble dynamics in subcooled flow boiling, Int. J. Heat Fluid Flow 25 (2004) 149–158.
[13] D.E. Maddox, I. Mudawar, Single- and two-phase convective heat transfer from smooth and enhanced microelectronic heat sources in a rectangular channel, ASME J. Heat Transfer 111 (1989) 1045–1052.
[14] H. Honda, H. Takamastu, J.J. Wei, Enhanced boiling of FC-72 on silicon chips with micro-pin-fins and submicron-scale roughness, ASME J. Heat Transfer 124 (2002) 383–389.
[15] J.J. Wei, H. Honda, Effects of fin geometry on boiling heat transfer from silicon chips with micro-pin-fins immersed in FC-72, Int. J. Heat Mass Transfer 46 (2003) 4059–4070.
[16] H. Honda, J.J. Wei, Enhanced boiling heat transfer from electronic components by use of surface microstructures, Exp. Therm. Fluid Sci. 28 (2004) 159–169.
[17] C. Ramaswamy, Y. Joshi, W. Nakayama, W.B. Johnson, Effects of varying geometrical parameters on boiling from microfabricated enhanced structures, ASME J. Heat Transfer 125 (2003) 103–109.
[18] K.N. Rainey, S.M. You, S. Lee, Effect of pressure, subcooling, and dissolved gas on pool boiling heat transfer from microporous, square pin-finned surface in FC-72, Int. J. Heat Mass Transfer 46 (2003) 23–25.
[19] Y.M. Lie, J.H. Ke, W.R. Chang, T.C. Cheng, T.F. Lin, Saturated flow boiling heat transfer and associated bubble characteristics of FC-72 on a heated micro-pin-finned silicon chip, Int. J. Heat Mass Transfer 50 (2007) 3862–3876.
[20] S.G. Kandlikar, Heat transfer characteristics in partial boiling, fully developed boiling, and significant void flow regions of subcooled flow boiling, ASME J. Heat Transfer 120 (1998) 395–401.
[21] Z.Y. Bao, D.F. Fletcher, B.S. Haynes, Flow boiling heat transfer of Freon R11 and HCFC123 in narrow passages, Int. J. Heat Mass Transfer 43 (18) (2000) 3347–3358.
[22] Y. Fujita, Y. Yang, N. Fujita, Flow boiling heat transfer and pressure drop in uniformly heated small tubes, in: Proceedings of the Twelfth International Heat Transfer Conference, vol. 3, 2002, pp. 743–748.
[23] S.J. Kline, F.A. McClintock, Describing uncertainties in single-sample experiments, Mech. Eng. 75 (1953) 3–12.
[24] C.O. Gersey, I. Mudawar, Effects of orientation on critical heat flux from chip arrays during flow boiling, ASME J. Electron. Packag. 114 (1992) 290–299.
[25] A. Ma, J. Wei, M. Yuan, J. Fang, Enhanced flow boiling heat transfer of FC-72 on micro-pin-finned surfaces, Int. J. Heat Mass Transfer 52 (2009) 2925–2931.